

# Influence of pre-existing damages on the degradation behavior of crystalline silicon photovoltaic modules

Christian Camus,<sup>1</sup> Ayodeji Adegbenro,<sup>1</sup> Jakob Ermer,<sup>1</sup>

Vignesh Suryaprakash,<sup>1</sup> Jens Hauch,<sup>1</sup> and Christoph J. Brabec<sup>1,2</sup>

<sup>1</sup>ZAE Bayern, Renewable Energies Division, Immerwahrstr. 2, 91058 Erlangen, Germany

<sup>2</sup>Materials for Electronics and Energy Technology (*i-MEET*),

Friedrich-Alexander-Universität Erlangen-Nürnberg, Martenstraße 7,  
91058 Erlangen, Germany

(Received 15 August 2017; accepted 2 December 2017; published online 21 March 2018)

In this paper, the influence of pre-existing crystalline damage, such as cracked or broken cells or soldering failures, as they are frequently observed in operating photovoltaic (PV) plants, on the degradation behavior of mono- and polycrystalline silicon PV modules is investigated. In particular, it is analyzed if and to what extent pre-damage introduced prior to lamination propagates upon stress exposure. Therefore, the pre-damaged modules are exposed to various accelerated aging conditions in order to analyze the impact of the pre-damage on the degradation behavior under the respective aging scenario. In order to separate the influence of the pre-damage from composition-induced influences, the choice of materials used in the modules is varied. These investigations reveal that none of the accelerated aging tests causes any change in the pre-existing damage. In fact, the degradation behavior and rate rather depended on the choice of the module components than on the nature of the pre-damage. Finally, these results are compared with indoor and outdoor results obtained from other studies. Published by AIP Publishing. <https://doi.org/10.1063/1.5000294>

## I. INTRODUCTION

Photovoltaics (PV) has become one of the major renewable energy sources. In 2016, a cumulative installed PV capacity of at least 303 GWp was in operation, of which 75.4 GWp have been newly installed in 2016.<sup>1</sup> In order to economically contribute a significant amount of energy to the global energy demand, the modules of these systems need to reliably generate electricity for 20 years or longer. In order to do so, low degradation rates are essential. Jordan *et al.*<sup>5</sup> determined a median annual degradation rate of 0.5%–0.6% for crystalline silicon-based PV modules, which constitute the vast majority of global installations.<sup>1</sup> The actual reasons leading to this degradation are manifold, and care must be taken when distinguishing between failures and degradation (see Ref. 2 and references therein). Whilst failures correspond to a sudden decrease in module power, degradation describes a rather continuous decay. However, the evolution of the performance of PV modules under real operating conditions usually constitutes a superposition of numerous (rather small) sudden effects which can have an immediate influence on the module performance (e.g., crack formation or breakage of preexisting cracks upon mechanical impact) and continuous aging effects (e.g., encapsulant browning and contact corrosion). In particular, cracks and cell fracture are phenomena frequently observed in operating PV plants.<sup>3,4</sup> However, as long as cracks do not lead to isolated cell areas or to a significant increase in the cell resistance, they only have a negligible effect on the module power.<sup>4,5</sup> Although many studies investigated the formation and propagation of cracks during production, transportation, installation, and operation<sup>6–10</sup> as well as the aging behavior of PV modules,<sup>11–14</sup> very little is known about the influence of damage caused by a sudden event on the further aging process of PV modules. Some work of ISFH analyzed the influence of cracks on the power loss after humidity-freeze (HF) aging, but crack propagation itself was not studied in detail.<sup>15,16</sup> Van Mölken *et al.*<sup>17</sup> and Schmauder *et al.*<sup>18</sup> conducted some analysis on the

influence and propagation of cracks on single pre-cracked solar cells in the lab, but so far no work addressed this aspect at the module level for field or accelerated aging lab conditions. Therefore, here, we expose PV modules made from cells with pre-existing cracks to various accelerated aging conditions and characterize them periodically to monitor the propagation of the damage as well as the degradation process itself.

## II. EXPERIMENTAL PROCEDURE

### A. Artificial aging

The modules are aged in three CTS C + 10/200 climate chambers under damp heat (DH), humidity-freeze (HF), and thermal cycling (TC) conditions. Experimental conditions for scenarios follow IEC 61215 Ed. 1 (1993), if not mentioned otherwise. However, some modifications, which are explained in detail below, are made since the purpose of this study is rather to identify a specific degradation behavior than qualifying a product. All tests are interrupted for less than 6 h (according to IEC DTS 62876-2-1 draft technical specification) once every 1–2 weeks for module characterization. Rarely, longer periods of up to 4 weeks are unavoidable due to non-availability of metrology systems.

For this study, two DH campaigns with durations of 156 days ( $\sim 3763$  h) and 141 days ( $\sim 3396$  h) are conducted. The duration deliberately exceeds the duration specified in the standard in order to continue testing until a clear differentiation between the ongoing degradation modes can be made.

The HF test procedure is conducted similar to IEC 61215 Ed. 1 (1993) with simplified temperature and humidity profiles: Humidity is only controlled at a temperature of  $85^{\circ}\text{C}$ . When the temperature is ramped from  $0^{\circ}\text{C}$  to  $-40^{\circ}\text{C}$ , the system is given 5 min to reach  $-40^{\circ}\text{C}$  without a specified rate, and when it is ramped from  $-40^{\circ}\text{C}$  to  $25^{\circ}\text{C}$ , a constant rate of  $41.5^{\circ}\text{C}/\text{min}$  is applied. This profile applies a comparable, if not harsher, stress profile so that the impact of the pre-damage on module degradation can be assessed. Here, a total of 127 cycles (1 cycle: 1354 min) is applied.

For TC, 642 cycles (1 cycle: 317 min) in total.

### B. Module properties

For this study, a set of 24 crystalline silicon (twelve poly-crystalline and mono-crystalline each) PV modules are produced in an industrial module manufacturing line using the manufacturer's standard processes. All modules have been produced as 6-cell modules ( $530\text{ mm} \times 350\text{ mm}$ , See Fig. 1) in the glass/ethylene vinyl acetate (EVA)/Si/EVA/backsheet configuration and equipped with standard junction boxes. Some of the cells (cell type "P2," see e.g., Poly 6) contain laser-passivated areas, which are visible as circular or oval black areas. These are not considered as damage within the framework of this study. For 18 of these modules (Poly 1–9 and Mono 1–9), cell cracks and cell fractures [i.e., cracks lead to isolated areas or form areas of increased resistance; these areas are visible as dark areas in electroluminescence (EL) images] are manually introduced prior to lamination by slowly applying mechanical pressure with a metal tip onto the cell surface until cracks are formed. If needed, the procedure is repeated several times at adjacent positions in order to obtain a series of damage forming damage with the desired orientation. This procedure is meant to mimic damage as it may be induced during wafer, cell, or module production before lamination.<sup>19,20</sup> For these modules, three kinds of damage are distinguished: (i) crack parallel to the busbar, (ii) crack perpendicular to the busbar, and (iii) cell fracture. Furthermore, for six modules (Poly 10–12 and Mono 10–12), two of the contact ribbons are incompletely soldered in order to mimic a soldering failure. In order to investigate, if the aging behavior is dominated by the nature of the pre-existing damage or by the module composition, the choice of components is varied throughout the set of modules. In particular, the cell type and the EVA front and back sheets, which directly influence the mechanical and chemical stabilities, are varied. Thus, it can be determined if modules of similar pre-damage or those of equal

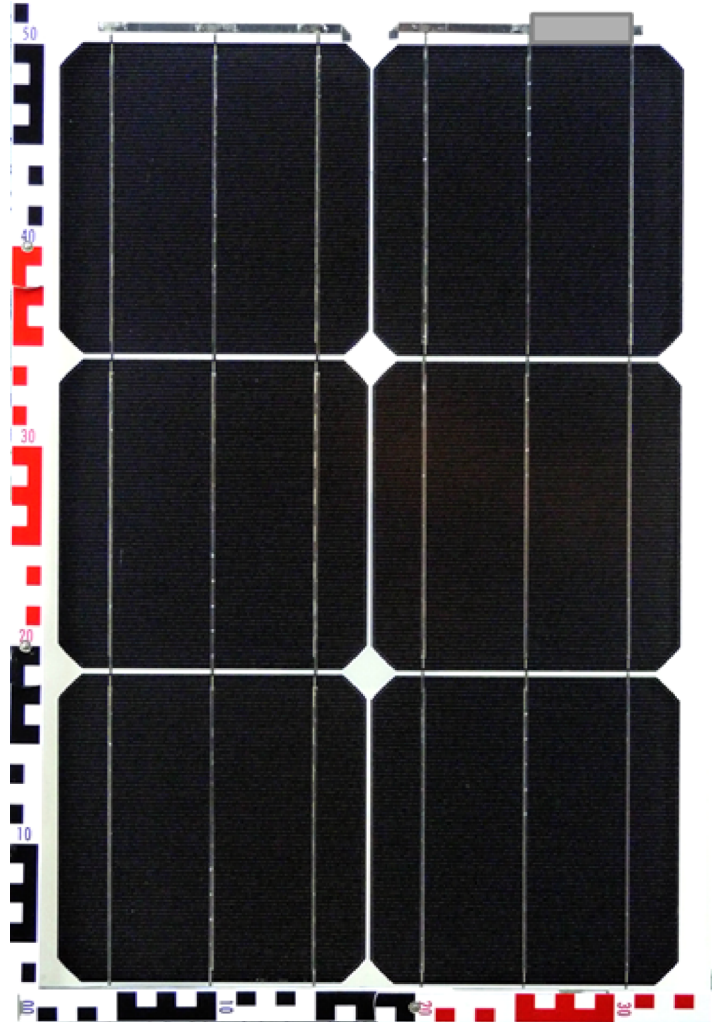


FIG. 1. Photograph of one of the modules produced for this study (mono-crystalline). A scale bar illustrates the module dimensions in cm. The grey box is inserted intentionally for covering the manufacturer label.

composition will exhibit a similar aging behavior. Table I summarizes the properties of the modules investigated in this study.

With respect to module power, all modules exhibit a power value of about 25 W under standard test conditions (STC, 25 °C, 1000 W/m<sup>2</sup>, AM1.5 spectrum) as determined using an AAA table flasher (Sec. II C). The poly-crystalline modules show an average power of 25.7 W, whereas for the mono-crystalline ones, the average power is determined to be 26.6 W. Under weak light conditions (200 W/m<sup>2</sup>), the average power for poly-crystalline modules is 5.1 W, whilst 5.4 W is measured for mono-crystalline modules. In Fig. 7, the power values of all modules at STC and weak light conditions are plotted (see the “initial state”).

### C. Electrical characterization

All modules are characterized using a Spire AAA flasher SPI-Sun Simulator 4600SLP with an AM1.5 spectrum. Measurements are performed at both STC and weak light conditions (200 W/m<sup>2</sup>). The pulse lengths are 40 ms at STC and 100 ms at 200 W/m<sup>2</sup>. All measurements are conducted in four-point geometry in order to reduce contact resistance losses. The modules are brought into contact by directly connecting to the contact ribbons in the junction box.

TABLE I. Summary of all modules exposed to accelerated aging. The aging scenario (DH: Damp-Heat, HF: Humidity-Freeze, and TC: Thermal Cycling), the initial damage, and the choice of module components are stated.

Test module	Test module description					
	Initial damage description	Material	Test condition	Cell type	EVA front	EVA back
Poly 1	Crack parallel to the busbar	Poly	DH	P2	EF1	EB1
Poly 2	Crack perpendicular to the busbar	Poly	DH	P1	EF1	EB1
Poly 3	Fractured cell	Poly	DH	P2	EF1	EB1
Poly 4	Crack parallel to the busbar	Poly	HF	P1	EF1	EB1
Poly 5	Crack perpendicular to the busbar	Poly	HF	P1	EF1	EB2
Poly 6	Fractured cell	Poly	HF	P2	EF1	EB1
Poly 7	Crack parallel to the busbar	Poly	TC	P2	EF1	EB1
Poly 8	Crack perpendicular to the busbar	Poly	TC	P1	EF1	EB2
Poly 9	Fractured cell	Poly	TC	P2	EF1	EB1
Poly 10	Soldering failure	Poly	DH	P1	EF1	EB1
Poly 11	Soldering failure	Poly	DH	P1	EF1	EB1
Poly 12	Soldering failure	Poly	DH	P2	EF1	EB3
Mono 1	Crack parallel to the busbar	Mono	DH	M1	EF1	EB1
Mono 2	Crack perpendicular to the busbar	Mono	DH	M1	EF1	EB1
Mono 3	Fractured cell	Mono	DH	M1	EF1	EB1
Mono 4	Crack parallel to the busbar	Mono	HF	M1	EF1	EB1
Mono 5	Crack perpendicular to the busbar	Mono	HF	M1	EF1	EB1
Mono 6	Fractured cell	Mono	HF	M1	EF1	EB1
Mono 7	Crack parallel to the busbar	Mono	TC	M1	EF1	EB1
Mono 8	Crack perpendicular to the busbar	Mono	TC	M1	EF1	EB1
Mono 9	Fractured cell	Mono	TC	M1	EF1	EB1
Mono 10	Soldering failure	Mono	DH	M3	EF3	EB4
Mono 11	Soldering failure	Mono	DH	M3	EF3	EB4
Mono 12	Soldering failure	Mono	DH	M3	EF3	EB4

#### D. Electroluminescence imaging

Electroluminescence (EL) images are conducted in a dark chamber using a greateyes GE 2048 2048 FI camera with a silicon detector (resolution:  $2048 \times 2048$  pixels). All images are obtained by applying a forward bias of 75% of the data sheet module  $I_{SC}$  (6.9 A) to the modules. The camera is set to an exposure time of 10 s. Also for this measurement, the modules are brought into contact by directly connecting to the contact ribbons in the junction box.

For all EL measurements, the final image is obtained by subtracting a background image (no current injection) from the image obtained under forward bias for noise reduction.

#### E. Thermographic imaging

All thermography measurements are conducted in a dark chamber in the Dark Lock-In Thermography (DLIT) mode. An IRCAM Equus 327kNM camera is used for DLIT containing a CMT detector of a resolution of  $640 \times 512$  pixels. For DLIT, a rectangular (5 s/7 A; 5 s/0 A) lock-in signal is applied. Three periods were recorded for one image. Also for this measurement, the modules are brought into contact by directly connecting to the contact ribbons in the junction box.

### III. RESULTS

#### A. EL analysis: Progression of module degradation

In Fig. 2, the EL images of the initial and final state of all modules are shown. Practically, all modules are affected by the accelerated aging. The modules that are exposed to TC aging

exhibit the smallest change according to their EL images, whereas for all modules exposed to DH and HF, significant changes in the images are observed. Figure 2 shows that very different degradation patterns occur within the set of modules. These EL degradation patterns and their progression will be discussed in greater detail in this paper.

First, it needs to be noted that all modules under investigation pass test durations as they are required in IEC 61215 Ed. 1 (1993) (1000 h DH, 10 cycles HF, 200 cycles TC) without failures.

For DH aging, first changes in the EL images are observed after approximately 2500 h of aging for most of the modules (Poly 1–3, Mono 2, and Poly 10–12). For these modules, the first

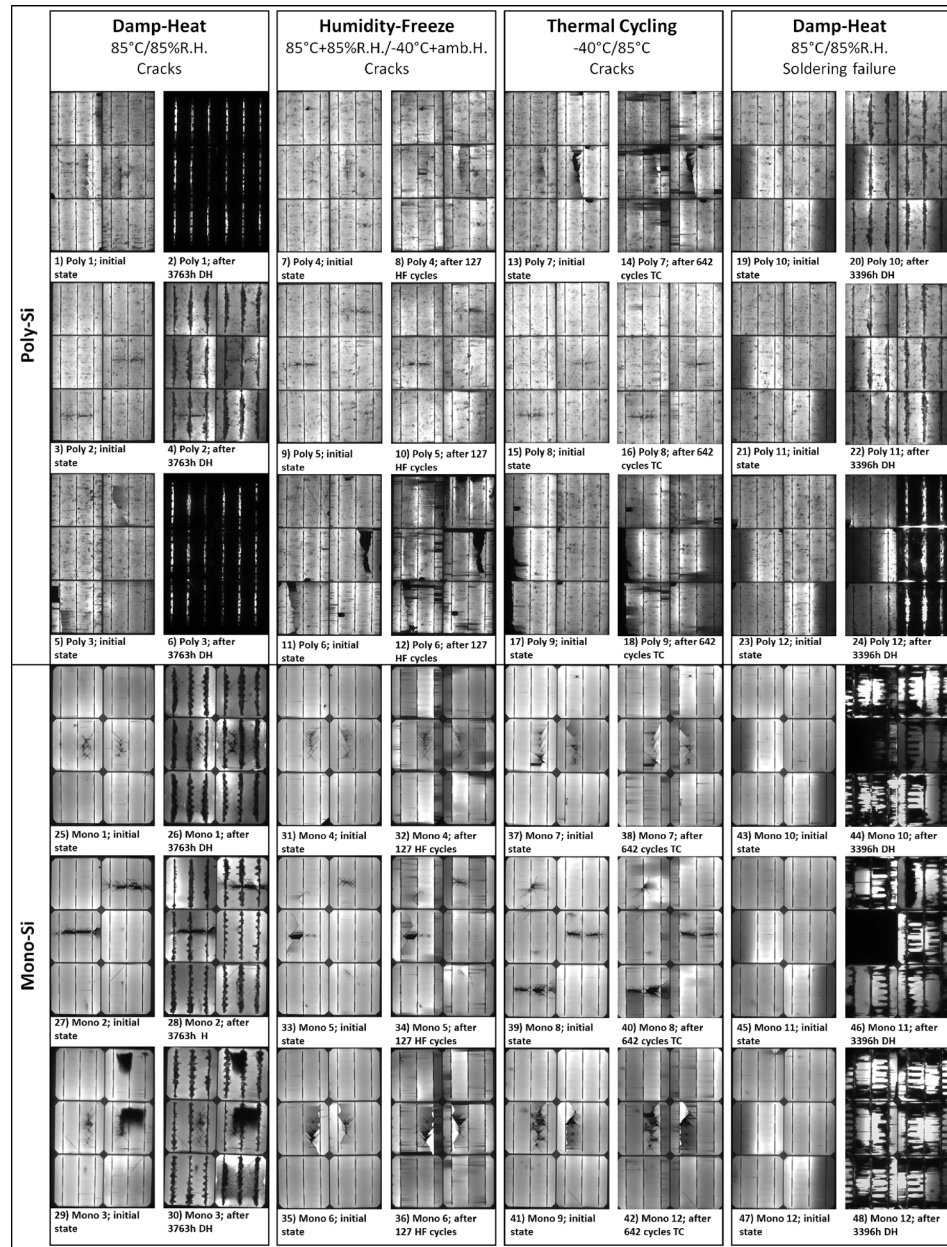


FIG. 2. Comparative EL (see Sec. II D for experimental details) images of all investigated modules. For each module, the initial and final states after completion of the respective test are shown. In total, twelve polycrystalline (images 1–24) and 12 mono-crystalline (images 25–48) are tested. Of those, 18 (nine poly and nine mono) exhibit various crack patterns and six (three poly and three mono) have solder failures introduced.

onset of degradation in EL is indicated by dark areas, initiating and spreading out from some point along the busbars. A second group of modules (Mono 10–12) shows first signs of degradation after a significantly shorter period of approximately 720 h of DH aging. Furthermore, module Poly 3 shows dark spots appearing in the active cell area which are not located at the busbars as a first sign of degradation already after 96 h. For Mono 3, a large-area greyish darkening of the cell area is observed after approximately 1300 h. Afterwards, further corrosion starting at the busbars also occurs after approximately 2500 h as for the other modules under DH aging. A peculiar behavior is observed for Poly 12: Here, half of the cells exhibited a degradation behavior that was significantly different from the other half, which is likely to be due to a batch-to-batch variation of cells of two different batches from the same manufacturer which are used in this module.

For modules Poly 1, Poly 3, Poly 12, Mono 10, Mono 11, and Mono 12, the degradation rate increases steadily after first initiation. In order to give a coarse quantification of the progression rate, the EL images are evaluated by a simple image analysis using ImageJ.<sup>21</sup> For the sake of reproducibility and comparability, all images are binarized with respect to their intensity applying a threshold value of 0.5 (with 0 being 100% black and 1 being 100% white). Then, the percentage of the black area is quantified and considered as the degradation-affected or “dead” area. Following this procedure, the progression of degradation can be visualized as it is exemplarily shown in Fig. 3 for Mono 10. Here, after initially moderate degradation progression, the rates accelerate as aging proceeds (here, after 1500 h).

For the same module, Mono 10, a sequence of exemplary EL images are shown in Fig. 4 together with the corresponding IR images recorded at the same stages of aging. Even though all the cells of the module exhibit similar degradation patterns, they affect the cells differently. At 1236 h, only a very small area is affected by degradation [see Fig. 4(g)]. Nevertheless, the IR image, which is still similar for all cells at 216 h [Fig. 4(a)], except for the defective contact ribbons, starts to develop different degradation patterns: Whilst cells 1, 5, and 6 are affected such that current flow concentrates on the cell parts without visible degradation, in cells 2, 3, and 4, hot spots evolve at positions strongly affected by degradation and lead to a strong concentration of heat emission at these locations. During the following aging steps, this trend becomes even more pronounced. By the end of the aging procedure, cell 3 appears almost completely shunted and also cell 4 is largely reduced in EL emission. Thus, it appears that in spite of similar appearance, this kind of degradation can affect the cells differently.

For the modules exposed to HF conditions, degradation is mainly visible by a moderate increase in broken contact fingers, leading to characteristic parallel dark areas perpendicular to

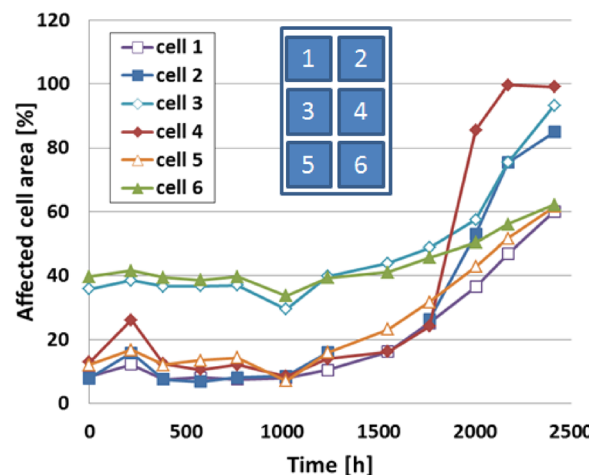


FIG. 3. Evolution of the progression of module degradation for module Mono 10. The plot depicts the area considered as the “dead area” by threshold-based image analysis of the EL images. The inset shows the order of cell numbering. Cells 2 and 6 were the ones with one incompletely soldered contact ribbon. Thus, image processing already yields a higher “dead area” at the beginning of the test.

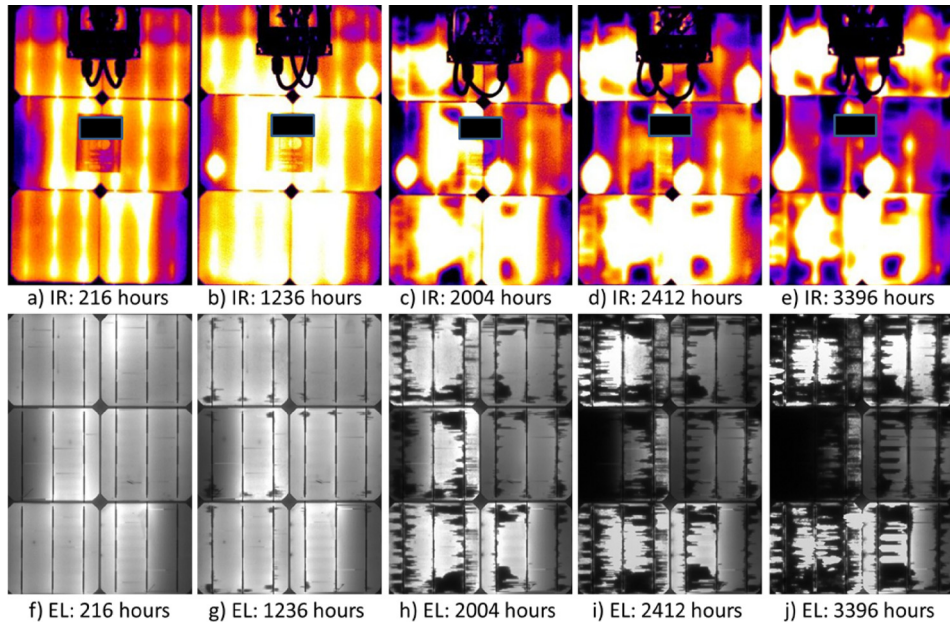


FIG. 4. Comparative IR and EL images of Mono 10: (a)–(e) IR images of a module after the indicated duration of DH testing. Images are recorded from the backside and are therefore mirrored at the long edge in order to facilitate comparability with EL images. In the IR images, the manufacturer label is covered by a black box. The junction box with cables is visible in the top center. The apparently “colder” part at the upper module edge is due to an additional foil which is applied here by the manufacturer. (f)–(j) EL images of the same module after the same aging durations in DH.

the busbars. Only, for Poly 6, a first onset of degradation similar to DH degradation is observed at the upper edge of cell 2, which initiates already after 28 cycles but only starts to expand after 113 cycles.

During TC aging, a constant increase in the number of broken contact fingers is observed throughout the aging. Beyond this, no further signs of degradation are observed in EL.

### B. EL analysis: Pre-damage propagation

Interestingly, for none of the modules exhibiting cracks (Poly 1–9 and Mono 1–9), any change in the crack pattern is observed by EL. Neither the orientation of the crack nor the composition, the aging scenario, or the technology of the particular module lead to deviations from this behavior. In Fig. 5, the evolution of the pre-damaged modules and cells is shown exemplarily for Poly 2, Poly 6, and Poly 8. It can be seen from the enlarged cell images that no change in the crack pattern occurs. The increase in the dark areas around the cracks for Poly 6 does not constitute a modification of the crack pattern but is only due to additionally electrically isolated areas caused by broken contact fingers.

In contrast, the modules with soldering failures exhibit failures of two of the cells with pre-damaged soldering joints. However, unexpectedly, these cells seem to be shunted instead of being electrically isolated. The heat distribution in Fig. 4(e) clearly shows that the current flows through a single point of one of the busbars. The same effect is observed for the shunted cell in Mono 11 (not shown). How far these shunts are connected to the initial soldering failure will be discussed in Sec. IV.

### C. Classification of degradation patterns

Based on the EL results stated above (Fig. 2), the degradation behavior was classified into four classes which are shown in Figs. 6(a)–6(h) and described in the following.

Poly 1, Poly 3, and half of Poly 12 finally reach a degradation level under DH conditions at which almost the entire cell area is completely degraded, i.e., it only shows a negligible

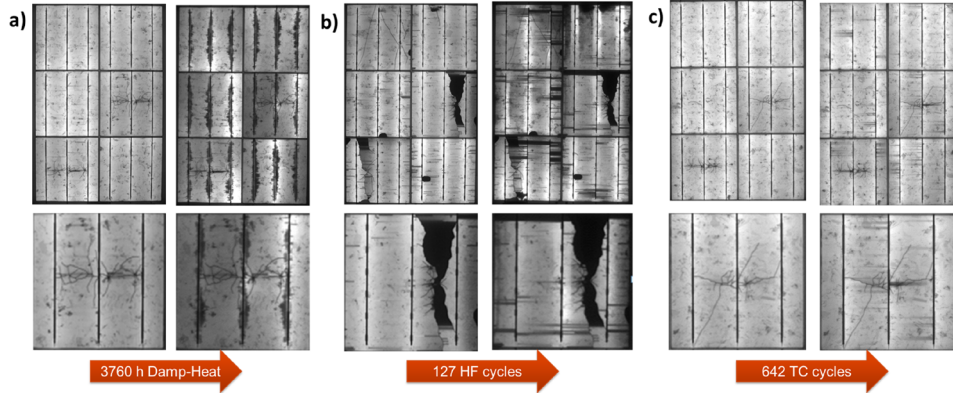


FIG. 5. Visualization of the static crack patterns throughout the aging process. For each module, the initial (upper left) and final (upper right) state EL images are shown. Additionally, an enlarged image of a cell affected by the respective crack pattern is shown (lower left and right). It can be seen that under none of the aging scenarios, any changes in the crack pattern are observed. Here, Poly 2, Poly 6, and Poly 8 are shown as representative examples. Comparable results are obtained for all modules under investigation.

intensity in the EL images. If at all, only a very small region right around the busbars retains a noticeable EL intensity in the final state. The EL image of this degradation mode “full area degradation” is shown in Fig. 6(a). In contrast, for Poly 2, Poly 10, Poly 11, half of Poly 12, and Mono 1–3, even at the end of the DH aging study, only a very small area around the busbars is affected by degradation. As this degradation behavior has been attributed to corrosion products of solder flux in Refs. 12–14 and 22, it is labeled as the “flux pattern busbar” [Fig. 6(b)]. Similarly, the degradation behavior of Mono 10–12 exhibits solder-flux-corrosion-like patterns. However, here, the degradation proceeds much faster and degradation is more severe.

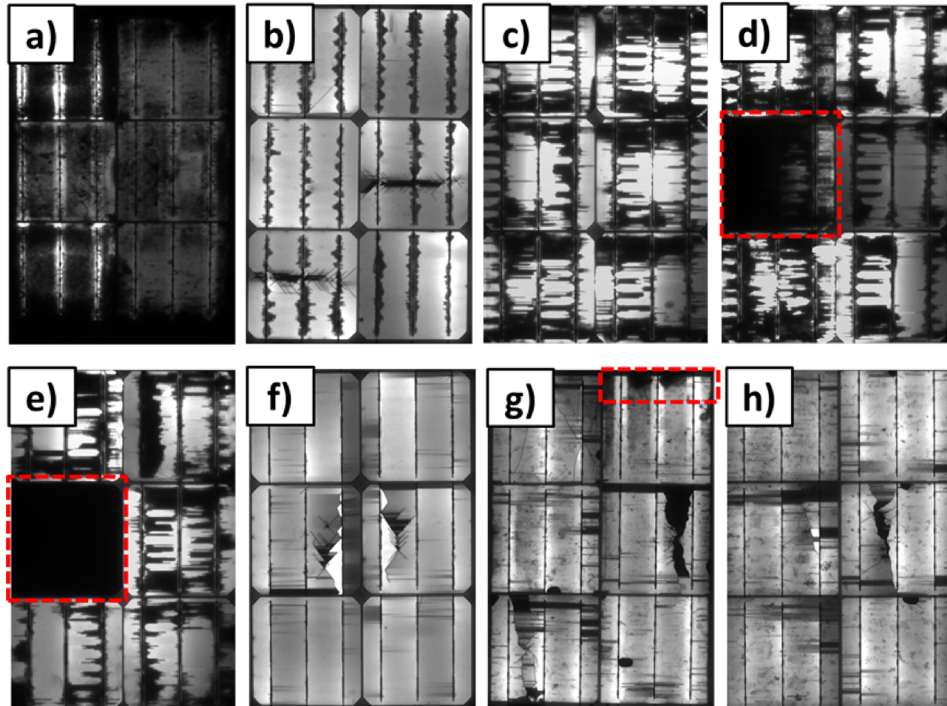


FIG. 6. Defect patterns observed in the aging tests: (a) full area cell degradation (DH), (b) flux pattern busbar (DH), (c)–(e) flux pattern busbar + fingers without (c) and with partially (d) and fully (e) shunted cells (DH), and (f)–(h) broken contact fingers without (f) and with (g) onset of cell degradation as obtained from HF and from TC (h).

TABLE II. Description of the effect of various degradation classes that were defined based on EL images on the electrical performance of the modules.

Degradation mode	Electrical parameter affected	Comment
Full area cell degradation	$FF$ and $I_{SC}$	
Flux pattern busbar	$FF$	
Flux pattern busbar + fingers	$FF$ , $I_{SC}$ , and $V_{OC}$	Minor effect on $V_{OC}$
Broken contact fingers (HF)	$FF$ (HF only)	No effect measurable for TC aging for any parameter

Since for this mode, degradation appears to progress from the busbars along the contact fingers, it was classified as “flux pattern busbar + fingers” [Fig. 6(c)]. In Figs. 6(d) and 6(e), the same pattern is seen, but here additionally, a partial (d) and full (e) shunting of the cell was observed. As it is likely that the shunting is rather due to the soldering failures than to the DH aging, these degradation modes were not classified as own classes. The fourth class “broken contact fingers” summarizes all modules with broken contact fingers as the dominant degradation mode. Here, two modifications are observed: The majority of modules aged under HF and TC conditions merely exhibit an increased number of broken contact fingers [Poly 4–5 and Mono 4–6, Fig. 6(f)], as well as all modules exposed to TC, Fig. 6(h)], whilst Poly 6 additionally shows first signs of DH-like degradation under HF conditions.

#### D. Electrical analysis

In this section, the changes in the electrical properties of the modules upon aging are discussed. Generally, the module power follows the degradation trends observed in EL measurements although usually degradation becomes visible in EL before an effect is observed in IV measurements. Therefore, this section is limited to the discussion of the overall reduction in module power upon accelerated aging. These losses are depicted in Fig. 7 for STC and weak light conditions. In all cases, the fill factor  $FF$  is affected the most during degradation. In severe cases of degradation, the short circuit current  $I_{SC}$  also decreases significantly but usually delayed with respect to  $FF$  degradation. Very rarely, the open circuit voltage  $V_{OC}$  is also affected. Table II summarizes the electrical parameters which decrease the most during degradation for the different failure classes.

These results agree well with the EL observations for TC and HF. Based on EL measurements, one would expect only a small or negligible effect of the aging experiments on module power. This is clearly confirmed by the IV measurements since neither under STC nor under weak light conditions, a significant loss in power is observed for any of the modules exposed to TC even though post-aging measurements under STC tend to show slightly lower powers than before testing.

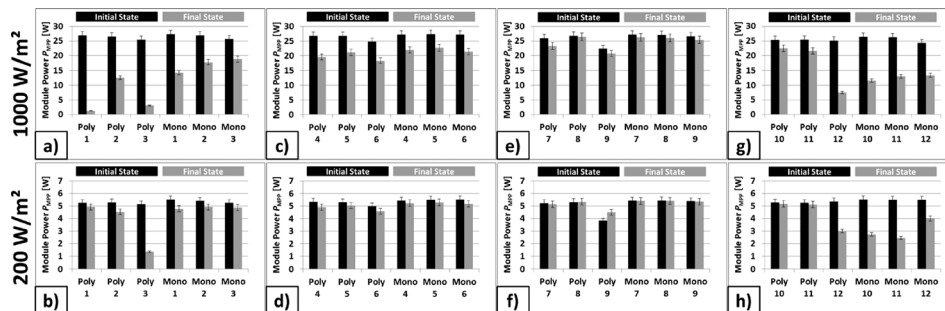


FIG. 7. Comparative IV measurements of all modules, at both STC (AM 1.5,  $1000 \text{ W/m}^2$ ,  $25^\circ\text{C}$ ) and weak light conditions (the same but  $200 \text{ W/m}^2$ ). (a) and (b): Poly 1-3 and Mono 1-3 (DH, cracks), (c) and (d): Poly 4-6 and Mono 4-6 (HF, cracks), (e) and (f): Poly 7-9 and Mono 7-9 (TC, cracks), and (g) and (h): Poly 10-12 and Mono 10-12 (DH, soldering failure).

For HF, a clear reduction in module power, exclusively caused by a reduction in *FF*, of about 5–7 W under STC is observed. For the mono-crystalline modules, this reduction is slightly lower than that for the poly-crystalline ones. Generally, the same trend is observed under weak light conditions, even though the reduction is much less significant here and falls within the margin of uncertainty of the measurements.

As for EL measurements, the strongest degradation is observed under DH conditions. The electrical measurements confirm the usefulness of the classification chosen based on EL as modules of one class also generally show a similar electrical degradation behavior.

Modules Poly 1, Poly 3, and Mono 10–12 show the most severe degradation which agrees well with EL observations. However, also module Poly 2 shows a very strong degradation which is—at first—surprising based on EL measurements as the degradation pattern is more similar to the one of Poly 10–11 or Mono 1–3, which exhibit much lower power losses. Most of this difference is presumably due to the slightly longer aging test duration of Poly 2 compared to modules Poly 10–11. After an aging period of 3192 h (compared to 3396 h for Poly 10–11), Poly 2 still has a module power of 20 W which is comparable to the final level of Poly 10–11.

Furthermore, IV measurements also reveal that in the final state, Mono 10–12 exhibit similar electrical parameters, even though a degradation of  $V_{OC}$ , which is minor for Mono 10 and Mono 12, is not yet observed for Mono 11. In particular, the shunted cells do not lead to major differences in module performance compared to Mono 12.

Another observation is that generally, relative power losses are much smaller under weak light conditions than under STC. Even a severely degraded module like Poly 1 only loses <10% of its weak light performance. In contrast, Poly 3 which behaves very similar to Poly 1 under STC shows a much higher loss under weak light, even though this loss is not as severe as under STC.

## IV. DISCUSSION

### A. Stability of cracks under accelerated aging conditions

The fact that, under none of the tested scenarios, any propagation of the pre-existing cracks occurs appears unintuitive at least for HF and TC aging as these scenarios are known to impose a significant amount of thermal stress on the modules.<sup>23</sup> In the following, the results will be compared with observations made by others and the fact how far this behavior can be explained will be discussed.

Kumar and Kumar<sup>24</sup> observed a significant increase in cracks in previously undamaged modules. In particular, they observed this increase if more than 300 cycles of TC were applied. Similar results were obtained by Philipp,<sup>25</sup> who reported that 50% of the modules tested at Fraunhofer ISE exhibited 3 or more new cracks after 200 cycles of TC. However, in the same report, the author also showed that even after 400 cycles of TC, 10% of the modules did not show any additional cracks. These results show that modules, if engineered well, can withstand several hundred cycles of TC without initiating any new cracks. However, none of these authors commented on the further propagation of pre-existing cracks or of cracks that were initiated early in the test.

For HF testing, which was reported by Philipp as the dominant failure reason during module certification,<sup>25</sup> several studies have been published by Kajari-Schröder *et al.*<sup>15,16</sup> In particular, the behavior of modules having been pre-damaged in a mechanical load test under subsequent HF testing was discussed. Here, the authors observed that the number of cracks after mechanical loading (i.e., prior to HF) is correlated with the power losses after 200 cycles of HF testing. This is attributed to the formation of electrically isolated areas which are formed between the cracks initiated by the mechanical load and which lead to the reduction of the active cell area. The same effect is also observed in the present study (e.g., isolated areas in Poly 6). The authors do not comment on the actual propagation of the cracks during HF testing. However, the EL images in Refs. 15 and 16 indeed show no crack propagation either. The observed isolated areas always form between the crack lines that were already visible prior to

HF testing, even though they had not been isolated at that stage. Such a formation of isolated cell areas is also observed in the present work (see, e.g., Poly 6 and Mono 6 or for TC, Poly 7), but here, it is also found in areas where no crack is observed (see, e.g., area right of the right busbar of the three cells in the left column of Poly 6). This indicates that the isolated area is actually caused by the increase in the number of broken contact fingers. Thus, the cracks only contribute indirectly to this effect by increasing the probability that a broken contact finger coincides with a crack line and thereby contributes to the formation of an isolated area. Nevertheless, also by this indirect contribution, the number of preexisting cracks can indeed influence the final power loss after HF aging. However, in the present study, no correlation between the number and the orientation of pre-existing cracks on the post-HF power loss is observed.

In the following, a coarse estimation of the maximum stresses that can be induced by HF testing is made in order to relate these results to mechanical load tests in which cracks are known to be initiated for loads above 2000 Pa.<sup>4</sup> Kempe<sup>26</sup> determined the solubility of water in typical PV EVA foil to be  $\sim 6 \times 10^{-5} \text{ g/cm}^3$  at 85°C. For an EVA thickness of 300 μm, this would mean that 1 cm<sup>2</sup> of EVA foil would be saturated with  $1.8 \times 10^{-6} \text{ g}$  of water. Even if this water would freeze completely once the test temperature drops below the freezing point of water, it would lead to a thermal expansion of only  $0.8 \times 3 \times 10^{-4} \text{ cm}^3 = 2.4 \times 10^{-4} \text{ cm}^3$ . Thus, it may be assumed that due to the rather low solubility of water in EVA, crack propagation is unlikely to be promoted. In order to further elucidate the reasons for the absence of crack propagation, the stresses caused by the thermomechanical changes of the materials during TC and HF shall be discussed. Eitner<sup>27</sup> analyzed the stresses in the cell plane for standard (uncracked) crystalline silicon PV modules. His studies revealed that whilst being relaxed at the lamination temperatures of  $\sim 150^\circ\text{C}$ , stresses of the order of 10<sup>7</sup> Pa, which are quantitatively comparable to stresses introduced by mechanical load testing of 2000 Pa or higher,<sup>4</sup> are introduced in the cell plane when cooling down to  $-40^\circ\text{C}$ . However, as it turns out that these stresses are compressive, they will not lead to the propagation of cracks, as it was observed in the present study. Similar findings have also been obtained by Paggi *et al.*<sup>28</sup> In particular, it needs to be taken into account that EVA's stiffness is much higher at low temperatures due to an increase in elastic modulus.

One peculiarity of the present study that needs to be taken into account is that here, cracks are introduced after stringing and prior to lamination. Thus, it can be assumed that the pre-cracked cells are laminated in a completely stress-free state. Thus, compressive stresses may be expected at all temperatures below the lamination temperature. In the field, this situation may vary a lot from case to case depending on the temperature of the cells while they are cracking, e.g., cells being cracked due to a snow load may carry a completely different stress compared to ones that are being cracked due to stresses introduced by the mounting unit at a high operating temperature of 70°C. This may explain, besides engineering aspects, why observations of crack propagation during TC and HF testing vary so strongly. Furthermore, stresses might have been lower for the six-cell-modules investigated here than for full-size modules analyzed by others due to smaller module dimensions.

Whilst Refs. 15 and 16 discussed the impact of cracks initiated in the finished module, studies investigating the impact of cracks initiated prior to lamination are rare. Grunow *et al.* introduced seed cracks of half the wafer depth into as-cut wafers, which were then laminated onto glass and stressed in a mechanical bending test and subsequently by TC testing.<sup>29</sup> Whereas mechanical bending led to a crack initiating at the seed crack, no changes in the crack pattern were observed during TC as it was observed here. In contrast to Ref. 29, Wendt *et al.* investigated solar cells that were soldered under inappropriate conditions so that flaking and small cracks were induced.<sup>30</sup> These cells were then processed to modules and stressed by 250 cycles of TC and 10 cycles of HF. In these tests, damage including crack growth was observed already after 50 TC cycles, which is in contrast to the observations of the present study. This is likely due to the fact that even though introduced prior to lamination, the damage in Ref. 30 was not stress-free, as stress might have been “frozen” by the soldering. Hence, it becomes clear that

the stress state of a pre-existing crack, which is determined by the circumstances of its initiation, needs to be taken into account when assessing its severity.

Finally, it needs to be noted that the observation of the absence of crack propagation under DH, TC, and HF conditions agrees well with field results of Buerhop *et al.*<sup>4,31</sup> who monitored modules with pre-existing cracks of unknown stress-state installed in the field in southern Germany during the course of one year with moderate fall and winter conditions (only one strong storm, no deep frost) and found that hardly any crack propagation occurred under these moderate conditions. In the same study, the authors also showed by lab in-situ mechanical load experiments that no significant crack generation occurs for mechanical loads below 2000 Pa.<sup>4</sup>

## B. Correlation of degradation behavior and module composition

For the modules exposed to TC and HF, similar observations were made for almost all modules, even though the composition is varied (see Table I). All these modules use EF1 as front EVA. However, two different back EVA films are used, and also, the cell type is varied for the polycrystalline modules. For all of them, the number of broken contact fingers increased during aging. Thus, the breaking behavior of the contact fingers does not seem to be determined by the module composition, i.e., by the choice of its components, which seems to be understandable as the stability of the fingers is likely to be determined by the choice of the paste used and the parameters of the printing process, which were both identical for all modules.

Poly 6 is the only module showing first signs of a DH-like cell degradation at the end of the HF test, and in fact, it is the only one containing cells of type P2, which also show fatal degradation under DH conditions (see discussion below). However, as it is the only module of this composition, it remains unclear, if this behavior is due to the properties of cell type P2 or if the module itself constitutes an outlier. Generally, it needs to be noted that the aging behavior under HF conditions agrees with the behavior observed under DH conditions. For the aging conditions applied here, the HF test conditions resemble DH conditions for 88% of the test time. Taking this into account, the onset of the first signs of DH-like degradation for Poly 6 roughly corresponds to the first appearance of signs of degradation of the same cell type under DH conditions.

For DH aging, the situation is more complex as various degradation patterns are observed. These are discussed and correlated with the module composition in the following.

Degradation pattern “full area cell degradation” is observed for Poly 1, Poly 3, and Poly 12, even though for Poly 12 only 50% of the cells are affected. Figure 8 displays the EL images for “full area cell degradation” for Poly 1. It becomes clear that at no stage of degradation, this degradation pattern is similar to the degradation pattern “flux pattern busbar,” in which areas of lower EL intensity form in the vicinity of the busbar. Therefore, both patterns constitute different degradation modes.

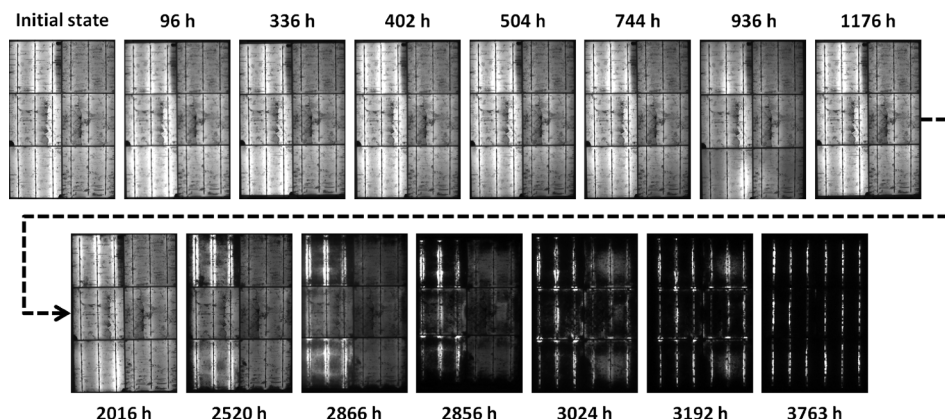


FIG. 8. Series of all EL images recorded for Poly 1. The evolution of the degradation (pattern “full area degradation”) can be followed after first signs of degradation after 2520 h. From this point, EL emission is increasingly concentrated on the direct vicinity of the busbars.

Degradation pattern “*full area cell degradation*” agrees well with observations of cells and modules affected by moisture-induced corrosion of the metallic silver grid.<sup>32</sup> In particular, for cells 2, 4, and 6, the characteristic “nebula-like” signature<sup>33</sup> of this failure mode can be seen in the EL images recorded after 3024 h and 3192 h. Also the electrical behavior of the affected modules, for which a severe reduction of *FF* followed by *I<sub>SC</sub>* is measured, agrees well with the observations in Ref. 32 and references therein. This degradation has been shown to be due to the progressive underetching of the silver grid fingers caused by the dissolution of the glass layer by acetic acid formed by the hydrolysis of the EVA encapsulant.<sup>32,34</sup>

From Table I, it can be seen that all three modules exhibiting degradation pattern “*full area cell degradation*” contain cells of type P2. Front EVA EF1 is used for all of them, whilst EB1 is used for Poly 1 and Poly 3 as back EVA whereas EB3 is used for Poly 12. As mentioned above, P2 is also the cell type used in the only module that showed DH-like degradation under HF conditions. Thus, it may be concluded that the appearance of “*full area cell degradation*” is due to the use of cells of type P2, which seem to be more prone to DH degradation than P1, showing less severe degradation of different appearance in both EL and electrical characterization measurements.

The degradation pattern “*flux pattern busbar*” has also been reported in the literature<sup>12–14,20,32,33</sup> to occur under DH conditions, and it is argued that this failure type is likely to be observed under real-world conditions due to a high activation energy.<sup>14</sup> Even though the details of the relevant process are not understood in detail, the phenomenon is known to be due to a chemical reaction between the soldering metallization and acetic acid stemming from the EVA encapsulation and favorably takes place under DH conditions.<sup>13,34</sup> Pingel *et al.* clearly showed that the degradation rate of this degradation pattern can be influenced significantly by the choice of the solder flux for otherwise identical modules.<sup>35</sup> It is thus assumed that the pH value of the solder flux is a dominant factor, if cells are prone to this degradation mode.<sup>22,35</sup> However, Pingel *et al.*<sup>35</sup> and Whitfield *et al.*<sup>13</sup> showed that the choice of cells and encapsulants is also of paramount importance for the occurrence of this degradation pattern. Based on these studies, it appears that this degradation can only occur under DH conditions for certain combinations of cells and solder flux. If the combination of both components is prone to this degradation pattern, the actual rate seems to be determined by the quality of the encapsulation, and it controls the amount of moisture which will finally provide the required acidic environment. Therefore, this degradation pattern can be concluded to exhibit certain similarities to the degradation pattern “*full area cell degradation*,” as in both cases, the metallic contacts are corroded in moisture-induced acidic environments. However, whereas for “*full area cell degradation*,” acetic acid is formed by the hydrolysis of the EVA and mainly attacks the silver grid line/cell interface, the pH value of the solder flux seems to be responsible for forming an acidic environment attacking the soldering/cell interface right at the busbar.

Here, modules Poly 2, Poly 10, Poly 11, and Mono 1–3 exhibit this degradation pattern. For these modules, EF1 and EB1 are used as EVA front and back foils, respectively. Obviously, different kinds of cells (P2, M1) are used. However, as the degradation pattern “*full area cell degradation*” is also observed for modules containing EF1 and EB1, it seems to be reasonable to identify the cell type as the critical component determining whether “*full area cell degradation*” or “*flux pattern busbar*” is observed as the dominant degradation pattern for the solder flux used in this study, which is identical for all modules.

For modules Mono 10–12, a degradation pattern similar to the degradation pattern “*flux pattern busbar*” is observed, but here the degradation is much more detrimental as it is not just limited to the direct vicinity of the busbar but apparently spreads out along the contact fingers and thus leads to a much larger affected area and occurs much earlier during DH testing. Additionally, fully or partially shunted cells are observed for the class “*flux pattern busbar + fingers*.” As mentioned above, the shunting of the cells might be due to the soldering failures leading to higher loads on the remaining contact ribbons during EL, IR, and IV measurements. The fact that the current flow is reduced to a single point of the affected solder tab during degradation (Fig. 4) indicates that the shunting might actually be a consequence of the soldering failure. Nevertheless, further studies on a larger set of modules with soldering failures

would be needed in order to elucidate this question in greater detail. The detrimental flux pattern degradation that is observed for these modules again correlates with a common composition of the affected modules which differs from the composition of modules exhibiting different degradation patterns. For modules Mono 10–12, EF3 and EB4 are used as EVA front and back foils, respectively, and M3 is chosen for the cell type. In comparison to the modules exhibiting the degradation pattern “*flux pattern busbar*,” this indicates that either M3 is even more prone to this degradation behavior for the given choice of solder flux or that the encapsulant used in these modules allowed for the ingress of more moisture so that degradation could propagate further from the busbars along the finger grid lines. Thus, it can be concluded that the degradation pattern “*flux pattern busbar + fingers*” constitutes a more severe case of the degradation pattern “*flux pattern busbar*,” whereas the degradation pattern “*full area cell degradation*” constitutes a kinetically and chemically different degradation mode.

In order to fully analyze the influence of the particular module components on the occurrence of a specific degradation mode, further investigations on a larger set of modules would be needed in the future. However, as mentioned above, here, the modification of module composition is mainly meant to serve as a cross-check to distinguish between the influence of certain pre-damage and the module composition. Based on the results presented in this study, the degradation behavior seems to be dominated by the module composition. In contrast, pre-existing cracks or breakages do not seem to influence the degradation pattern. Merely, the existence of soldering failures may lead to an increased likelihood for cell shunting.

### C. Further observations

One striking result of this study is the only moderate power loss of the modules under weak light conditions even for modules that lost almost 100% of their power under STC conditions. This is a strong indication that degradation mainly affects the contacts but not the semiconductor itself. Following Ohm’s law, the impact of a high contact resistance  $R_{\text{cont}}$  on the module or cell power  $P$  becomes low for low currents  $I$ , i.e., low irradiation  $E$ :  $P = U \times I = R \times I^2$ , with  $I$  being proportional to  $E$ . In cases of shunting, the opposite effect would be expected.<sup>36</sup> This also agrees with the observations that mainly the fill factor is affected in this study and that in DH, mainly the grid fingers or the busbar is attacked. In this context, the observation that, for DH conditions, a strong dependence of the losses on the choice of solar cells was observed would thus rather indicate a more or less pronounced pre-deposition of the respective cell/metal interface for this kind of degradation than a degradation of the semiconductor itself (Poly 1 and Poly 3). However, at this point, this effect cannot be studied in greater detail and will need further analysis in the future in order to test this explanation.

## V. CONCLUSION

The results of this study indicate that pre-damage such as cracks and soldering failures only has a negligible influence on the degradation behavior of the affected modules. In all cases, the degradation behavior is predominantly determined by the composition of the modules, i.e., by the choice of components. For cracks, no crack propagation is observed under any of the test conditions, which may be explained by the presence of solely compressive stresses for temperatures below the lamination temperature which is the case for all accelerated aging scenarios discussed here. In the case of soldering issues, it seems likely that the presence of this damage may favor the shunting of the affected cells during DH aging.

Generally, the results of this study indicate that under moderate conditions, i.e., the absence of singular events such as strong storms or snow loads, no propagation of pre-existing cracks in PV modules may be expected, which agrees well with observations made in the field.

## ACKNOWLEDGMENTS

The research project “Smart Grid Solar” was co-financed by the European Union through the European Regional Development Fund and by the Free State of Bavaria.

- <sup>1</sup>International Energy Agency, “Snapshot of global photovoltaic markets 2016,” Report IEA PVPS T1, IEA, 2017.
- <sup>2</sup>G. TamizhMani and J. Kuitche, *Accelerated Lifetime Testing of Photovoltaic Modules* (Solar America Board for Codes and Standards, 2013).
- <sup>3</sup>C. Buerhop-Lutz, D. Schlegel, C. Vodermayer, and M. Nieß, “Quality control of PV-modules in the field using infrared-thermography,” in *26th European Photovoltaic Solar Energy Conference, Hamburg, Germany* (2011), pp. 3894–3897.
- <sup>4</sup>C. Buerhop, S. Wirsching, S. Gehre, T. Pickel, T. Winkler, A. Bemm, J. Mergheim, C. Camus, J. Hauch, and C. J. Brabec, “Lifetime and degradation of pre-damaged PV-modules - Field study and lab testing,” in *44th IEEE Photovoltaic Specialist Conference, Washington D.C., USA*, 2017.
- <sup>5</sup>D. C. Jordan, T. J. Silverman, J. H. Wohlgemuth, S. R. Kurtz, and K. T. VanSant, “Photovoltaic failure and degradation modes,” *Prog. Photovoltaics* **25**, 318–326 (2017).
- <sup>6</sup>M. Köntges, M. Siebert, A. Morlier, R. Illing, N. Bessing, and F. Wegert, “Impact of transportation on silicon wafer-based photovoltaic modules,” *Prog. Photovoltaics* **24**, 1085–1095 (2016).
- <sup>7</sup>A. M. Gabor, M. Ralli, S. Montminy, L. Alegria, C. Bordonaro, J. Woods, L. Felton, M. Davis, B. Atchley, and T. Williams, “Soldering induced damage to thin Si solar cells and detection of cracked cells in modules,” in *21st European Photovoltaic Solar Energy Conference, Dresden, Germany* (2006), pp. 2042–2047.
- <sup>8</sup>H. Xiong, C. Gan, Z. Hu, H. Niu, J. Li, J. Si, P. Xing, and X. Luo, “Formation and orientational distribution of cracks induced by electromagnetic induction soldering in crystalline silicon solar cells,” *IEEE J. Photovoltaics* **7**(4), 966–979 (2017).
- <sup>9</sup>G. Mathiak, L. Pohl, J. Sommer, U. Fritzsche, W. Herrmann, F. Reil, and J. Althaus, “PV module damages caused by hail impact - Field experience and lab tests,” in *31st European Photovoltaic Solar Energy Conference and Exhibition, Hamburg, Germany* (2015), pp. 1915–1919.
- <sup>10</sup>G. Mathiak, J. Sommer, W. Herrmann, N. Bogdanski, J. Althaus, and F. Reil, “PV module damages caused by hail impact and non-uniform snow load,” in *32nd European Photovoltaic Solar Energy Conference and Exhibition, Munich, Germany* (2016), pp. 1692–1696.
- <sup>11</sup>N. G. Dhere, “Reliability of PV modules and balance-of-system components,” in *31st IEEE Photovoltaic Specialists Conference, Lake Buena Vista, FL, USA* (2005), pp. 1570–1576.
- <sup>12</sup>P. Hacke, R. Smith, K. Terwilliger, S. Glick, D. Jordan, S. Johnston, M. Kempe, and S. Kurtz, “Testing and analysis for lifetime prediction of crystalline silicon PV modules undergoing degradation by system voltage stress,” in *38th IEEE Photovoltaic Specialists Conference, Austin, TX, USA* (2012), pp. 246–253.
- <sup>13</sup>K. Whitfield, A. Salomon, S. Yang, and I. Suez, “Damp heat versus field reliability for crystalline silicon,” in *38th IEEE Photovoltaic Specialists Conference, Austin, TX, USA* (2012), pp. 1864–1870.
- <sup>14</sup>P. Hacke, M. Kempe, K. Terwilliger, S. Glick, N. Call, S. Johnston, S. Kurtz, I. Bennett, and M. Kloos, “Characterization of multicrystalline silicon modules with system bias voltage applied in damp heat,” in *25th European Photovoltaic Solar Energy Conference and Exhibition, Valencia, Spain* (2010), pp. 3760–3765.
- <sup>15</sup>M. Köntges, I. Kunze, S. Kajari-Schröder, X. Breitenmoser, and B. Bjorneklett, “Quantifying the risk of power loss in PV modules due to micro cracks,” in *25th European Photovoltaic Solar Energy Conference, Valencia, Spain* (2010), pp. 3745–3752.
- <sup>16</sup>S. Kajari-Schröder, I. Kunze, and M. Köntges, “Criticality of cracks in PV modules,” *Energy Procedia* **27**, 658–663 (2012).
- <sup>17</sup>J. I van Mölken, U. A. Yusufoglu, A. Safiei, H. Windgassen, R. Khandelwal, T. M. Pletzer, and H. Kurz, “Impact of micro-cracks on the degradation of solar cell performance based on two-diode model parameters,” *Energy Procedia* **27**, 167–172 (2012).
- <sup>18</sup>J. Schmauder, K. Kurz, and A. Schneider, “Controlled introduction of cracks into crystalline silicon solar cells and subsequent acoustic excitation,” *Energy Procedia* **77**, 407–413 (2015).
- <sup>19</sup>X. F. Brun and S. N. Melkote, “Analysis of stresses and breakage of crystalline silicon wafers during handling and transport,” *Sol. Energy Mater. Sol. Cells* **93**, 1238–1247 (2009).
- <sup>20</sup>P. Å. Wang, “Industrial challenges for thin wafer manufacturing,” in *4th IEEE World Conference on Photovoltaic Energy Conversion, Waikoloa, HI, USA* (2006), pp. 1179–1182.
- <sup>21</sup>See [imagej.nih.gov/ij/features.html](http://imagej.nih.gov/ij/features.html) for ImageJ-Image Processing and Analysis in Java, ImageJ Features.
- <sup>22</sup>M. D. Kempe and D. C. Jordan, “Evaluation and modeling of the potential effects of a module manufacturing anomaly,” *Prog. Photovoltaics* **25**(12), 982–988 (2017).
- <sup>23</sup>International Energy Agency - PVPS, “Review of failures of photovoltaic modules,” Report IEA-PVPS T13-01:2014, IEA, 2014.
- <sup>24</sup>S. Kumar and G. Kumar, “Analysis of effect of thermal cycling test on photovoltaic module using EL technique,” *Int. J. Adv. Eng. Res.* **3**(VI), 73–78 (2012).
- <sup>25</sup>D. Philipp, PV module reliability and quality testing, PV Investors Day, Rio de Janeiro, Brazil, 2015.
- <sup>26</sup>M. D. Kempe, “Modeling of rates of moisture ingress into photovoltaic modules,” *Sol. Energy Mater. Sol. Cells* **90**, 2720–2738 (2006).
- <sup>27</sup>U. Eitner, “Thermomechanics of photovoltaic modules,” Ph.D. thesis (Martin-Luther-University Halle-Wittenberg, 2011).
- <sup>28</sup>M. Paggi, I. Berardone, A. Infuso, and M. Corrado, “Fatigue degradation and electric recovery in Silicon solar cells embedded in photovoltaic modules,” *Sci. Rep.* **4**(4506), 1–7 (2014).
- <sup>29</sup>P. Grunow, P. Clemens, V. Hoffmann, B. Litzenburger, and L. Podlowski, “Influence of micro cracks in multi-crystalline silicon solar cells on the reliability of PV module reliability of PV modules,” in *20th European Photovoltaic Solar Energy Conference, Barcelona, Spain* (2005), pp. 2380–2383.
- <sup>30</sup>J. Wendt, M. Träger, M. Mette, A. Pfennig, and B. Jaeckel, “The link between mechanical stress induced by soldering and micro damages in silicon solar cells,” in *24th European Photovoltaic Solar Energy Conference, Hamburg, Germany* (2009), pp. 3420–3423.
- <sup>31</sup>C. Buerhop, S. Wirsching, A. Bemm, T. Pickel, P. Hohmann, M. Nieß, C. Vodermayer, A. Huber, B. Glück, J. Mergheim, C. Camus, J. Hauch, and C. J. Brabec, “Evolution of cell cracks in PV-modules under field and laboratory conditions,” *Prog. Photovoltaics* (published online).

- <sup>32</sup>International Energy Agency - PVPS, "Assessment of photovoltaic module failures in the field," Report IEA-PVPS T13-09:2017, 2017, pp. 43–49.
- <sup>33</sup>A. Masuda, N. Uchiyama, and Y. Hara, "Degradation by acetic acid for crystalline Si photovoltaic modules," *Jpn. J. Appl. Phys., Part 1* **54**, 04DR04 (2015).
- <sup>34</sup>A. Kraft, L. Labusch, T. Ensslen, I. Dürr, J. Bartsch, M. Glatthaar, S. Glunz, and H. Reinecke, "Investigation of acetic acid corrosion impact on printed solar cell contacts," *IEEE J. Photovoltaics* **5**(3), 736–743 (2015).
- <sup>35</sup>S. Pingel, H. Korth, M. Winkler, P. Weiss, and T. Geipel, "Investigation of damp heat degradation mechanisms and correlation to an accelerated test procedure (HAST)," in *27th European Photovoltaic Solar Energy Conference, Frankfurt, Germany* (2012), pp. 3137–3141.
- <sup>36</sup>P. Hacke, K. Terwilliger, and S. Kurtz, "In-situ measurement of crystalline silicon modules undergoing potential-induced degradation in damp heat stress testing for estimation of low-light power performance," in *23rd Workshop on Crystalline Silicon Solar Cells & Modules: Materials and Processes*, Breckenridge, Colorado, USA, 2013.